

---

**This manuscript is a preprint** and has not undergone peer-review. Subsequent versions of this manuscript may have different content. If accepted, the final version of this manuscript will be available via the '*Peer-reviewed Publication DOI*' link on the right-hand side of this webpage. Please feel free to contact any of the authors directly or to comment on the manuscript using **hypothes.is** (<https://web.hypothes.is/>). We welcome feedback!

---

1       How do tectonics influence the initiation and evolution of submarine  
2                   canyons? A case study from the Otway Basin, SE Australia

3                   Nan Wu<sup>1\*</sup>, Harya D. Nugraha<sup>2</sup>, Michael J. Steventon<sup>3</sup>, Guangfa Zhong<sup>1</sup>

4       <sup>1</sup>State Key Laboratory of Marine Geology, Tongji University, Shanghai 200092, China

5       <sup>2</sup>Center for Sustainable Geoscience, Universitas Pertamina, Jakarta, 12220, Indonesia

6       <sup>3</sup>Shell Research, Shell Centre, London, SE1 7NA, UK.

7       \*Email: [nanwu@tongji.edu.cn](mailto:nanwu@tongji.edu.cn)

8       **Abstract**

9       The architecture of canyon-fills can provide a valuable record of the link between tectonics,  
10       sedimentation, and depositional processes in submarine settings. We integrate 3D and 2D seismic  
11       reflection data to investigate the dominant tectonics and sedimentary processes involved in the  
12       formation of two deeply buried (c. 500 m below seafloor), and large (c. 3-6 km wide, >35 km long)  
13       Late Miocene submarine canyons. We found the plate tectonic-scale events (i.e. continental  
14       breakup and shortening) have a first-order influence on the submarine canyon initiation and  
15       evolution. Initially, the Late Cretaceous (c. 65 Ma) separation of Australia and Antarctica resulted  
16       to extensional fault systems, which then formed stair-shaped paleo-seabed. This inherited seabed  
17       topography allowed gravity-driven processes (i.e. turbidity currents and mass-transport complexes)  
18       to occur. Subsequently, the Late Miocene (c. 5 Ma) collision of Australia and Eurasia, and the  
19       resulting uplift and exhumation, have resulted in a prominent unconformity surface that coincides  
20       with the base of the canyons. We suggest that the Late Miocene intensive tectonics and associated  
21       seismicity have resulted in instability in the upper slope that consequently gave rise to  
22       emplacement of MTCs, initiating the canyons formation. Therefore, we indicate that regional  
23       tectonics play a key role in the initiation and development of submarine canyons.

24       Keywords: Submarine buried canyons; Mass-transport complexes; Canyon-fill; Tectonic activity

25       **1. Introduction**

26       Submarine canyons are ubiquitous in deep-water settings and have long been considered as one  
27       of the major conduits for transporting sediment from the shelf edge, across the continental slope,

28 and into the deeper abyssal plain (Shepard, 1981; Normark et al., 2003; Antobreh and Krastel,  
29 2006). They are normally characterised by U-shaped cross-sectional geometries, that represents  
30 incision of hundreds of metres into the underlying stratigraphy, extend for several kilometres in  
31 width, and up to hundreds of kilometres long (i.e. Lewis and Barnes, 1999; Baztan et al., 2005; Su  
32 et al., 2020). When buried, the coarse-grained canyon-fill (i.e. sand-rich turbidites) may act as  
33 reservoirs for hydrocarbons and/or long-term carbon storage, in many submarine settings (i.e. in  
34 the South China Sea, Gulf of Mexico, offshore West Africa, and SE offshore Australia; Moore et al.,  
35 2000; Posamentier and Kolla, 2003; Crossey et al., 2006; Gong et al., 2011; Su et al., 2014; Tassone  
36 et al., 2014). Submarine canyon-fills have been well studied from large-scale outcrop analogues,  
37 which provided valuable information on lithofacies, sedimentary processes, and depositional  
38 model of canyon-fills (i.e. Champion et al., 2003; Di Celma, 2011; Hodgson et al., 2011; Zecchin et  
39 al., 2011; Figueiredo et al., 2013). However, due to their limited exposures, it is difficult to  
40 thoroughly examine the three-dimensional sedimentological and architectural evolution of  
41 canyon-fills in the field. Seismic reflection data-based studies have contributed significantly to our  
42 understanding of the three-dimensional morphology, internal architecture and stratigraphic  
43 evolution of the buried canyons on the continental shelf (i.e. Rasmussen, 1994; He et al., 2013)  
44 and continental slope regions (i.e. Gong et al., 2011; Maier et al., 2018; Su et al., 2020). However,  
45 the previous canyon-fills related studies lack examples of deeply buried (i.e. > 200m) canyons that  
46 deposited in the deeper submarine settings (i.e. continental lower slope or abyssal plain, water  
47 depth > 200 m), leading to an incomplete assessment of the canyon-fills evolution and, therefore,  
48 are generally inadequate to resolve initiation and evolution of canyons in deep marine settings  
49 where water depth exceeds 200 m.

50 In this study, we focus on the Otway Basin, located on the south-eastern Australian margin (Figure  
51 1a). The modern seabed geometry is characterised by a low gradient ( $0.4^\circ$  to  $1^\circ$ ) continental shelf  
52 in the upper region, a steep ( $10^\circ$  to  $30^\circ$ ) continental slope that is transacted by multibranching  
53 canyons, and mass-transport complexes (MTCs) are also distributed in the middle slope, and a  
54 broad Southern Ocean abyssal plain (c. 5-7 km below seafloor) in the lower region (Figure 1b; Leach  
55 and Wallace, 2001; Wu et al., 2021b). The high-resolution 3D and 2D seismic reflection data from  
56 offshore SE Australia have provided us with a new opportunity to constrain buried canyons  
57 sedimentological and architectural evolution in submarine settings. In this study, we present two

58 deeply buried, isolated cut and fill canyons (BC-1 and BC-2) that were formed in the Late Miocene.  
59 We aim to investigate the architectural evolution and depositional processes from seismic facies  
60 analyses and infer potential links of canyon initiation and evolution to plate tectonic events. A  
61 detailed examination conducted in this study can provide valuable information to understand the  
62 evolutionary history of buried canyons in the abyssal plain and act as an analogue for comparison  
63 to other submarine canyons.

## 64 2. Geological setting

### 65 **2.1 Structural Framework**

66 The Otway Basin is an NW-striking rift basin located on the south-eastern South Australia passive  
67 margin (Figure 1a, 1b). The Otway Basin was initiated by rifting during the Late Jurassic to early  
68 Palaeogene and formed due to the eventual continental separation between Antarctica and  
69 Australia during the break up of Gondwana at the end of the Cretaceous (Figure 2; Willcox and  
70 Stagg, 1990; Perincek and Cockshell, 1995; Norvick and Smith, 2001; Krassay et al., 2004). Since  
71 the Jurassic, the Otway Basin has had two significant phases of extensional tectonism, including a  
72 Late Jurassic- Early Cretaceous rifting phase and a Late Cretaceous rifting phase (Perincek and  
73 Cockshell, 1995; Krassay et al., 2004). The post-rift stage of the Otway Basin commenced in the  
74 Late Cretaceous, and most of the major faulting and tectonic activities associated with the final  
75 separation of Australia and Antarctica Plate ceased at that time (Krassay et al., 2004; Holford et al.,  
76 2014). The Late Jurassic- Early Cretaceous rifting phase has created an intense faulting event that  
77 affects the entire Cretaceous succession (Figure 3; Moore et al., 2000). The Cretaceous faults are  
78 generally NW-SE striking normal faults with an average dip of 60° (Figure 3; Ziesch et al., 2017). The  
79 final breakup of the Australia and Antarctica Plates has resulted in a regionally distributed  
80 unconformity surface (Horizon H1 in this study; Figure 2, Figure 3) which separates the underlying  
81 Cretaceous and overlying Cenozoic successions (Krassay et al., 2004). These extensional faults  
82 normally terminate in the overlying thin Cenozoic succession and are characterised with high-angle  
83 extensional faults that dominant the shallower part of the basin, lower angle listric faults are  
84 common in the deeper part of the basin (Figure 3). During the Late Miocene to Early Pliocene, the  
85 collision between Australia and the subduction zones of the Indo-Australian plate has generated

86 long-wavelength (of the order  $10^3$  km) intraplate forces (Hillis et al., 2008; Tassone et al., 2012;  
87 Tassone et al., 2014). The Southern Australia margin has recorded this intraplate force and  
88 experienced an intensive uplift, exhumation and deformation (Figure 3; Dickinson et al., 2002;  
89 Sandiford, 2003; Hillis et al., 2008). The onset of this late Miocene tectonic phase is marked by a  
90 regional unconformity (Horizon H2 in this study; Figure 2) that is widely distributed along the deep-  
91 water sedimentary basins in SE Australia (Dickinson et al., 2002).

## 92 **2.2 Sedimentology**

93 The study interval lies in the Cenozoic stratigraphy in a passive continental margin setting. During  
94 the Cenozoic, the Otway Basin was in an open marine depositional environment, characterised by  
95 marine-related, calcareous-rich sediments (McGowran et al., 2004). The strata of the Cenozoic  
96 succession comprises of: the Wangerrip Group, the Nirranda Group, the Heytesbury Group, and  
97 the Whalers Bluff Formation (Figure 2; Perincek and Cockshell, 1995; Krassay et al., 2004; Totterdell  
98 et al., 2014). The Wangerrip Group (late Palaeocene to middle Eocene) represents the beginning  
99 of the passive margin sedimentation after the cessation of Late Cretaceous rifting (Figure 2). It  
100 unconformably overlies the regional Late Cretaceous unconformity (Horizon H1) and comprises of  
101 siliciclastic rich sediments (Figure 2). The Nirranda Group (middle Eocene to early Oligocene) is a  
102 succession of fine-grained siliciclastic in the lower section and marls in the upper section (Figure  
103 2). The Heytesbury Group (late Oligocene to late Miocene) is deposited in fully marine conditions  
104 dominated by a combination of calcareous mudstone and sandy limestone (Figure 2; Ziesch et al.,  
105 2017). The Late Miocene to Pliocene tectonic inversion induced the deposition of fluvial sands,  
106 which continues up to the present day (Norvick and Smith, 2001). The Whalers Bluff Formation  
107 (WBF, Pliocene-Recent; Figure 2) mainly consists of siliciclastic-rich sediments and is mostly  
108 developed near the continental slope area (Tassone et al., 2011).

## 109 **3. Dataset and Methodology**

### 110 **3.1 Dataset**

111 A Geoscience Australia Database is used as the primary data source for this work, including high-  
112 resolution 2D and 3D seismic reflection data (Figure 1b). The seismic reflection data encompass  
113 the modern continental shelf, continental slope, and abyssal plain area (Figure 1b). As shelf

114 progradation occurs seaward since Miocene times, the Miocene shelf edge is located c. 50 km  
115 landward of the modern shelf edge (Figure 1b; Leach and Wallace, 2001). Therefore, the seismic  
116 datasets provide the opportunity to investigate the evolutionary history of buried canyons and the  
117 tectonic features in the deep submarine setting. The 3D seismic-reflection dataset (OS02 3D)  
118 covers an area of c. 360 km<sup>2</sup>, with a bin spacing of 25 m × 12.5 m (inline × crossline). The 3D seismic  
119 data is zero-phase and presented in SEG normal polarity with an increase in acoustic impedance  
120 expressed as a positive amplitude (Figure 4). The dominant frequency within the stratigraphic  
121 interval of interest is c. 35 Hz, giving an average velocity of the buried sediment of 2450 m/s, and  
122 a vertical resolution of approximately 17.5 m.

### 123 **3.2 Methodology**

124 The age of the buried canyons was determined by correlations with offset wells (Figure 3) described  
125 in nearby studies (Leach and Wallace, 2001). We identified and interpreted three key horizons (H1,  
126 H2, and seabed), based on their high continuity (which extend throughout the study area) and  
127 strong amplitude. Horizon H1 (Figure 3, Figure 4) is a regionally mappable unconformity that has  
128 been correlated to the intra-Maastrichtian unconformity surface (Holford et al., 2014), and which  
129 records the eventual separation of the Australian and Antarctic Plates (Krassay et al., 2004; Holford  
130 et al., 2014). Horizon H2 (Figure 4, Figure 5) is another regionally mappable unconformity that  
131 defines the base of the Middle Miocene, which formed due to the tectonic uplift and the associated  
132 canyon erosion (Holdgate et al., 2000; Dickinson et al., 2001; Leach and Wallace, 2001).

133 Five seismic facies are identified based on their external geometry, internal configuration, seismic  
134 amplitude, continuity, and seismic reflection termination patterns (Figure 6). The seismic facies  
135 interpretation is further guided by comparing their expression with previous seismic facies analysis  
136 schemes developed for buried submarine canyon-fills in the nearby area (Leach and Wallace, 2001)  
137 and in similar basin settings (Mayall et al., 2006; Gong et al., 2011; Mauffrey et al., 2017; Maier et  
138 al., 2018). A variance (coherency) attribute was calculated to illustrate and delineate the  
139 morphology and internal structures of the intra-canyon depositional elements. Variance attribute  
140 calculates the variability of a trace to its neighbour over a particular sample interval and produces  
141 interpretable lateral changes in acoustic impedance (Van Bommel and Pepper, 2000), low variance  
142 response represents similar traces, and high variance response represents discontinuities (Brown,  
143 2011). Therefore, coupled with seismic facies analyses, variance attributes can contribute to better

144 imaging and mapping intra-canyon deposits.

## 145 4. Result

### 146 **4.1 Seismic facies**

#### 147 *Seismic facies-1: Turbidite complexes*

148 Seismic facies-1 (SF-1) consists of parallel to sub-parallel, continuous, high amplitude seismic  
149 reflections (Figure 6). SF-1 typically displays onlapping or pinching out geometries toward the  
150 canyon sidewalls (Figure 6). SF-1 can be observed in most of the canyon cross-sectional profiles, it  
151 comprises approximately 5-10% of the buried canyon stratigraphy. SF-1 is c. 60-90 m thick and  
152 preferentially occurs at the base of the canyon fill. It is abundant in the lower section of the buried  
153 canyons and becomes less obvious in the middle and upper sections. Based on the seismic  
154 characteristics and previous seismic facies-based studies, SF-1 is interpreted as primarily coarse-  
155 grained turbidite complexes, representing multiple episodes of turbidity currents deposition (i.e.  
156 Cross et al., 2009; Gong et al., 2011; Wu et al., 2021a).

#### 157 *Seismic facies-2: Background slope deposits*

158 Seismic facies-2 (SF-2) is characterised by sheet-like, medium- to low-amplitude, laterally  
159 continuous reflections that cap SF-1 and SF-3 (Figure 6). SF-2 consists of a flat base and top surface  
160 with fair cross-sectional continuity, and no erosive features have been observed. In general, the SF-  
161 2 preferentially occurs at the middle part of the canyon-fill, and makes up c. 20% of the buried  
162 canyon stratigraphy. The thickness of SF-2 is constant, ranging from 150-190 m. Based on the  
163 seismic characteristics and previous seismic facies-based studies, SF-2 is interpreted as a mix of  
164 fine-grained turbidite complexes and mud-rich hemipelagic deposits (Symons et al., 2017; Maier  
165 et al., 2018), representing a low-energy depositional environment (Prather et al., 1998).

#### 166 *Seismic facies 3: Mass transport complexes (MTCs)*

167 Seismic facies-3 (SF-3) consists of a discontinuous to chaotic reflection package with high- to  
168 medium-amplitude seismic reflections (Figure 6). The SF-3 is c. 170-300 m thick, has a rugose top  
169 surface and a relatively flat base surface (Figure 6). It dominates the middle to upper canyon-fill,  
170 representing nearly 60% of the buried canyon stratigraphy. The chaotic nature of the SF-3,  
171 combined with the rugose upper surface, indicates SF-3 has been remobilised and transported,  
172 mostly as MTCs (Prather et al., 1998; Posamentier, 2005; Maier et al., 2018). Based on its seismic

173 reflection character, we propose that SF-3 was initially deposited as and ultimately sourced from  
174 the remobilisation of SF-1 and SF-2.

#### 175 *Seismic facies 4: Turbidite channel*

176 Seismic facies-4 (SF-4) is defined by medium-high amplitude, and has a bowl-shaped external form  
177 with an erosional base (Figure 6). Internal reflections of SF-4 are characterised by chaotic, medium  
178 amplitude reflection. Seismic reflections outside the SF-4 are of fair continuity and medium-high  
179 amplitude reflections (Figure 6). The thickness of SF-4 ranges from 130-170 m, it is observed  
180 primarily in the upper section of the canyon-fill, representing c. 5% of the buried canyon  
181 stratigraphy. The internal amplitudes of SF-4 are higher than that of the surrounding seismic facies,  
182 which indicates a higher acoustic impedance contrast when compared with surrounding facies. The  
183 erosional nature at the base of SF-4 suggests incisions, and the high amplitude of the fill might  
184 suggest that SF-4 is dominated by sandstone-rich deposits. We interpret SF-4 as turbidite channel  
185 deposits, as indicated by studies from Perov and Bhattacharya (2011) and Posamentier and Kolla  
186 (2003).

#### 187 *Seismic facies 5: Contourite channel*

188 Seismic facies-5 (SF-5) is defined by sub-parallel to wavy, low-high amplitude seismic reflections,  
189 with truncated internal reflections (Figure 6). SF-5 can be easily recognised in the uppermost  
190 section of the buried canyons, near the continental shelf edge, having an elongated mounded  
191 shape and an adjacent concave moat (Figure 6). Based on its seismic reflection character, SF-5 is  
192 interpreted as contourites that are affected/reworked by contourite currents (Stow et al., 2002;  
193 Stow and Faugères, 2008; Rebesco et al., 2014).

### 194 **4.2 The buried canyons**

195 The buried canyons (BC-1 and BC-2) are deposited in the Oligocene to Miocene Heytesbury Group,  
196 and belong to Miocene Canyon systems which are defined by Leach and Wallace (2001). The BC-1  
197 and BC-2 oriented NNE-SSW, subparallel to the paleo-slope direction (Figure 7a, 7b). The BC-1 is  
198 broad U-shaped canyons in seismic cross-section, ranging from c. 3 km to 5 km wide and cutting  
199 approximately c. 300 m to 500 m deep (Figure 8a-d). It is bounded by a lower undulatory erosional  
200 surface (Horizon H2) that truncates the underlying strata, showing a distinct seismic amplitude  
201 with negative polarity (Figure 4, Figure 8). The U-shaped erosional surfaces represent the oldest  
202 period of erosion and can be identified on most of the canyon cross-sectional profiles. The canyon

203 sidewalls are steep, ranging from 20° to more than 30° (Figure 8). A series of sliding blocks are  
204 locally modified and truncated the steep canyon sidewalls, and located along the canyon margin  
205 (Figure 8c, 8d).

206 The seismic facies assemblage of the sliding blocks is similar and can be correlated to the  
207 undeformed strata adjacent to the canyon walls, and is therefore interpreted to fail along the  
208 canyon sidewalls (Figure 8d). After the formation of the U-shaped erosional canyon base, the  
209 accommodation is filled by several different seismic facies. Based on the seismic facies infill pattern  
210 and their location toward the slope, the BC-1 is divided into two transverse segments (Upper  
211 segment and Lower segment; Figure 7b). The Upper segment starts from the upper (NW) gap of  
212 the 3D seismic data to the lower edge of the paleo-slope. The Lower segment covers most of the  
213 3D seismic data area, expanding from the lower slope to the abyssal plain. In the following section,  
214 we take BC-1 (the biggest buried canyon in the study area) as an example to further investigate its  
215 facies association and infill patterns.

### 216 **4.3 Canyon architecture**

#### 217 *Upper segment*

218 The upper segment of the BC-1 truncates into the paleo-lower continental slope (Figure 7a, 7b).  
219 The maximum width and relief of the buried canyon is c. 3 km and 300 m, respectively. In this  
220 segment, the lowermost and the uppermost section of the buried canyon is commonly filled with  
221 SF-1, suggesting that turbidite complexes are the most dominant depositional elements during the  
222 initial and final phase of the buried canyon-fill (Figure 8a, 8b). The upper section of the buried  
223 canyon filled is commonly SF-2, suggesting that hemipelagic deposits are deposited shortly after  
224 the turbidite complexes (Figure 8a, 8b). In the uppermost part of the canyon-fill, the SF-5 are  
225 present, indicating the contourite current activities have influenced the final stage of the canyon-  
226 fill (Figure 8a).

#### 227 *Lower segment*

228 The Lower segment is SSW-oriented and constitutes the portion of the buried canyons where major  
229 accumulation took place. The width of the canyon in this segment is up to c. 7 km, with maximum  
230 sidewall reliefs of c. 500 m (Figure 8c, 8d). In the 3D seismic data area, most of the canyon-fill of  
231 the BC-1 is characterised by SF-3, which can constitute more than 70% of the canyon stratigraphy,  
232 with only thin (c. 30 m) deposition of SF-1 and SF-2 deposited in the middle or upper parts of the

233 stratigraphy (Figure 8c, 8d). Further downslope, regional 2D seismic lines image several other  
234 buried canyons that deposited in the deeper submarine setting, with the percentage of the SF-3  
235 infill increasing to nearly 90% of the total canyon stratigraphy (Figure 9a, 9b). The large percentage  
236 SF-3 infill show MTCs are the largest component of the Lower segment infill. A relatively thin fill (c.  
237 90 m to 200 m) of turbidite complexes and background slope deposits appears in the upper section  
238 of the buried canyons.

239 The thick accumulation of MTCs indicate the Lower segment represents the part of the buried  
240 canyons where the intensity of erosion reached its peak (Figure 9a, 9b). The lower section of the  
241 canyon-fill was likely eroded by MTCs and preserved as erosional remnants scattered throughout  
242 the canyon-fill lower section (Figure 8c). The presence of the erosional remnants indicates the  
243 erosive MTCs has been initiated and transported from the Upper segment, and ultimately  
244 deposited in the Lower segment where extensive erosion is normal.

#### 245 **4.4 Intra-canyon MTCs**

246 Several vertically stacked MTCs have been observed from the seismic sections cutting through the  
247 Lower segment of the BC-1. We map three seismically distinctive MTCs (MTC-1 to MTC-3; Figure  
248 8c, 8d) to investigate the morphological and kinematic properties of these intra-canyon MTCs.

249 MTC-1 is bounded by horizons H2.1 and H2.2, it is laterally confined by the canyon base surface  
250 (Horizon H2) and mainly consisting of chaotic seismic facies with high amplitude seismic reflections  
251 (Figure 8c, 8d). MTC-1 is 90 to 130 m thick, being thickest near the canyon centre, and progressively  
252 thins towards and onlaps onto the canyon sidewalls (Figure 8c, 8d). In plain view, the distribution  
253 of MTC-1 is spatially confined within the BC-1, the lateral margins of MTC-1 follow an NNE-  
254 orientated direction, coinciding with the orientation of BC-1 sidewalls (Figure 10a). MTC-2 is 120  
255 to 190 m thick and bounded by horizon H2.2 and H2.3, and it contains chaotic seismic facies with  
256 medium amplitude reflections (Figure 8c, 8d). The lateral margins of MTC-2 follows an NNE-  
257 orientated direction, subparallel to the orientation of canyon sidewalls. Similar to MTC-1, MTC-2 is  
258 laterally confined by the Horizon H2 and spatially distributed within the area of the BC-1 (Figure  
259 10b). MTC-3 is 130 to 210 m thick, and it is bounded by horizon H2.3 and H2.4, mainly consisting  
260 of chaotic seismic facies with medium amplitude reflections (Figure 7c, 7d). MTC-3 has NNE-  
261 orientated lateral margins, and the distribution of this MTC is nearly the same extent as the BC-1  
262 (Figure 10c).

263 The orientation of NNE-striking lateral margins suggests these MTCs were transported towards the  
264 SSE. Although there is no direct evidence indicating the source area of MTCs, the overall  
265 distribution (confined within the lower section of canyon-fills) and the nature of the seismic facies,  
266 together suggest MTC-1, MTC-2, and MTC-3 may derive from the failures of turbidite complexes or  
267 background sediments that originally deposited in the Upper canyon segment. The strictly confined  
268 nature of the intra-canyon MTCs indicates that the distribution of these failures is controlled by the  
269 canyons' morphology (i.e. the width and the height). Compared with MTC-1, the areal extent of  
270 MTC-2, and MTC-3 is larger, which suggests mass failure processes become more dominant with  
271 the evolution of canyon-fill. The vertically stacked deposition pattern of these MTCs suggests the  
272 intense erosion and sediment failure in the buried canyons were enhanced by tectonic deformation.  
273 The reoccurrence of the intra-canyon MTCs may be associated with the intensive faulting activities  
274 during Late Miocene–Pliocene fault reactivation, which has been variously ascribed to the  
275 contemporaneous collision of Australia's northern margin with the island arc in New Guinea (Hill  
276 et al., 1995).

## 277 5. Discussion

### 278 ***5.1 Sedimentological evolution of buried canyons***

279 Based on the canyon-fill pattern, the evolutionary model of the buried canyons identified in the  
280 Otway Basin can be summarised into three stages: (i) mass-transport complexes (MTCs) dominated  
281 the erosional stage, (ii) turbidites dominated the depositional stage, and (iii) an interbedded MTC-  
282 turbidite dominated erosional-depositional stage.

283 At the initial erosional stage, the morphology of the U-shaped canyon base has been attributed to  
284 the erosion by multiple mass failure events, as recorded by the thick deposition of MTCs in the  
285 distal section of the canyon-fill (Figure 9a, 9b). Another interpretation for the formation of the  
286 canyon base is the turbidity currents shaped the canyon and were then remobilised as MTCs. As  
287 turbidite complexes (or channel lags; Mayall et al., 2006) were observed at the lowermost section  
288 of the canyon-fill (Figure 9a). Due to the steep angle of the canyon sidewall (dips from c.40° to 60°),  
289 sidewall initiated sliding also occurs at the initial erosional stage. In the second depositional stage,  
290 processes such as turbidity currents and background sedimentations take place. The repeated

291 cutting and filling by turbidity currents is one of the major features of canyon-fill, and the canyon-  
292 fill remains stable, similar to depositional patterns that have been recorded in other fills (i.e.,  
293 Deptuck et al., 2007; Gong et al., 2011; Liang et al., 2020). In the final erosional-depositional stage,  
294 the canyon fill is dominated by the deposition of MTCs and turbidite channels. Contourite currents  
295 may play a role in the final stage of the canyon evolution. However, it is confined to the upper slope  
296 region, where the contourite currents are stronger than other current regimes (i.e. turbidity or  
297 mass-transport processes). For example, in the Upper segment of the canyon-fill (Figure 8a), the  
298 uppermost of the canyon-fill contains a large portion of contourite drifts and shows a distinct  
299 pattern similar to other area where contourite activities are intense (i.e. He et al., 2013; Warratz  
300 et al., 2019).

### 301 ***5.2 Origin of the buried canyons***

302 The causal mechanisms by which submarine canyons in the shallow submarine settings are  
303 initiated are generally a combination of near shelf-edge fluvial erosion during periods of relative  
304 sea-level fall/and or higher sediment flux (i.e. Posamentier et al., 1991) and retrogressive slope  
305 failure events occurring near the upper slope (i.e. Coleman et al., 1983; Goodwin and Prior, 1989;  
306 Pratson and Coakley, 1996; He et al., 2014). The strong contourite current, tidal current activities,  
307 and hurricanes and typhoons, that occur near the coast may also play a role in the canyon initiation  
308 (i.e. Shepard et al., 1974; Sequeiros et al., 2019).

309 In the study area, the oldest buried Miocene canyons are tied to occur near the base of the  
310 Heytesbury Group (Leach and Wallace, 2001). Therefore, the initiation of the buried canyons likely  
311 started during the Late Miocene, when cool-water carbonates dominated (Leach and Wallace,  
312 2001). The canyon bases are with high rugosity and show clear erosional features that are similar  
313 to those (i.e. grooves or scours) observed from the basal shear surface of MTCs (i.e. Bull et al., 2009;  
314 Butler et al., 2016). The Lower segment of the buried canyon-fill is characterised by a dominant  
315 deposition of MTCs, and the proportion of MTCs infill constantly increases toward to the farther  
316 distal part. Therefore, the origin of the buried canyons is tied to the occurrence of erosive gravity-  
317 driven processes (most likely mass failure events) during Late Miocene.

### 318 ***5.3 How do Late Miocene tectonics dictate the canyon initiation?***

319 During Miocene, the SE Australia margin has experienced an extremely intense episode of uplift  
320 event, where the study area has experienced the most (Dickinson et al., 2001; Dickinson et al.,

321 2002; Tassone et al., 2012). The driving mechanism for this uplifting episode is crustal shortening  
322 controlled intra-plate stresses, triggered by the northward movement of Australia towards the  
323 subduction zones along the northern boundary of the Indo-Australia plate (i.e. Sandiford, 2007;  
324 Hillis et al., 2008). Such a momentous uplift event has generated a significant net exhumation  
325 around the deep-water Otway Basin during Late Miocene. For example, the gross exhumation in  
326 the submarine Otway Basin is more than 1000 m during Late Miocene to Pliocene (Green et al.,  
327 2004), near the study area, the gross exhumation could reach more than 1500 m (Duddy, 1997;  
328 Tassone et al., 2014). The significant exhumation has created an increase in onshore sediment  
329 supply and elevated levels of seismicity in the continental region (Dickinson et al., 2001). These  
330 changes likely increased sediment instability in the upper slope and, consequently, gave rise to  
331 mass failure events (Sandiford, 2003; Sandiford et al., 2004). The above mentioned processes  
332 associated with the continental margin uplifting are marked by a regional erosion surface (Horizon  
333 H2 in this study) that can be traced for c. 1500 km along with SE Australia (Dickinson et al., 2002;  
334 Tassone et al., 2012). This is especially the case in the deep submarine where the regional erosion  
335 surface is corresponded to the extremely irregular canyon base surface (H2), and the canyon-fills  
336 are observed to display a thick package of chaotic seismic facies, indicating deposition of MTCs.  
337 The Late Miocene erosion period corresponds to the time when the entire shelf was exposed and  
338 thus heavily incised by frequent deposition of MTCs, that were transported down to the deeper  
339 part of the basin. We infer that mass failures during episodes of intense tectonic, rather than other  
340 factors, caused of incision on the continental slope to initiate the development of buried canyons.  
341 The Late Miocene tectonics have helped establish a mature sediment conduit system that  
342 extended from shallower marine down to the abyssal plain.

#### 343 ***5.4 How do Late Cretaceous tectonics influenced the canyon evolution?***

344 The late Cretaceous fault systems are generally NW-SE striking (Figure 11a, 11b; Ziesch et al., 2017).  
345 The dip- and cross-seismic sections have revealed these faults cutting vertically beneath the  
346 thalwegs of the BC-1 and BC-2 (Figure 4b, 5b, 9b). The seismic dip line along the canyon axis shows  
347 the presence of the faults has created a stair-shaped structure within the Lower segment, which is  
348 truncated by the canyon (Figure 5b, 9b). The seismic dip line along the area outside the buried  
349 canyons show that after deposition of the pre-canyon succession (sedimentation between horizon  
350 H1-H2), the paleo-seafloor (at the time of H2) may have inherited the geometry created by the

351 Cretaceous fault systems, showing a stair-shaped structure with a high-gradient (Figure 11c). This  
352 can be clearly seen from the onlapping patterns of sediments onto the local topographically high  
353 created by buried faults (Figure 11c).

354 The stair shaped geometry is interpreted as the hanging walls of the deeply sourced fault systems  
355 may have created a local structure high on the Late Cretaceous seafloor when horizon H1 is  
356 deposited. The footwalls of the deeply sourced fault systems have created a local structure low on  
357 the Late Cretaceous seafloor (Figure 12a). After the burial, the buried footwalls acted as a local  
358 high (buried hanging walls are locally low), causing an elevation difference between two adjacent  
359 footwalls and hanging walls (Figure 12a). When the canyon initiates, the stair-shape paleo  
360 geometry can cause an immediate increase in currents (e.g., turbidity currents or debris flow)  
361 energy and erosivity, thus facilitating the canyon development (Figure 12b). The subsequent  
362 canyon-fills was also influenced by the inherited topography created by the previous canyon infill  
363 and the stair-shape canyon base (Figure 12c). In modern analogues, the local gradient variation of  
364 the seabed has played a key role in canyon evolution (e.g., expansion in canyon width and depth),  
365 as demonstrated by modern canyon systems (Qin et al., 2017; Wu et al., 2021b). Therefore, we  
366 suggest that the late Cretaceous fault-controlled zones may have pre-determined the location of  
367 the canyons by facilitating the erosional downcutting during the formation of the canyon base, this  
368 influence has not been instantaneous, instead the impact on the canyon evolution can be felt as  
369 late as tens of million years (or more).

### 370 **5.5 Implication**

371 Previous studies show that the tectonically active settings tend to develop small-scale, short-lived  
372 canyons (Eyles and Lagoe, 1998), while canyons in tectonically stable passive margin settings tend  
373 to develop relatively large scale canyons which are active for longer periods (Coleman et al., 1983).  
374 However, we reveal that in the tectonically active regions, uplift and tilting due to tectonic  
375 deformation induce an increased in sediment supply and seismicity, which can promote mass  
376 failure events thus contribute significantly to the formation of large-scale submarine canyons.  
377 Therefore, we indicate that the factors which preconditioned and triggered mass-transport  
378 complexes can also induce canyon initiation and facilitate canyon development. We suggest that  
379 the plate tectonic scale events (i.e. continental breakup and shortening) have a first-order influence  
380 on the submarine canyon initiation and evolution. The impact from the regional tectonics to the

381 buried canyons can be instantaneous (i.e. directly trigger canyoning processes), or their influence  
382 can also be postponed (i.e. indirectly influence the seabed topography thus the canyon geometry).

## 383 6. Conclusion

384 1. The interpretation of the seismic data reveals that the sedimentological evolution of buried  
385 canyons can be divided into: (i) a mass-transport complex (MTC) dominated erosional stage, (ii) a  
386 turbidite dominated depositional stage, and (iii) a mixed MTC-turbidite dominated the erosional-  
387 depositional stage. We indicate that in the deeper submarine settings (i.e. lower continental slope  
388 or abyssal plain), the interplay of turbidity currents and mass failure events control the canyon  
389 sedimentological and architectural patterns.

390 2. The intimate association of the buried canyon base with the Late Miocene uplift events suggest  
391 that canyon inception was triggered by Miocene uplifting and associated upper slope instability.  
392 We suggest that repeated mass failure is the most likely driving mechanism of the buried canyon  
393 inception, in conjunction with increased sediment flux due to exhumation of the margin.

394 3. We interpret the extensional faults associated with the late Cretaceous plate separation  
395 between Australia and Antarctica as responsible for the inception and evolution of the buried  
396 canyons by increasing the steepness of the paleo-seabed, thus controlling the canyon geometry  
397 and location.

398 4. Plate-scale tectonic events have a close link with the submarine canyon initiation and evolution  
399 processes. The influence from regional tectonic movements to the initiation of canyons may have  
400 been almost instantaneous (i.e. directly triggering canyoning processes), or their influence can also  
401 be delayed (i.e. indirectly influence the canyon geometry).

## 402 Figure Caption

403 Figure 1. Location map of the study area. (a) Regional map of Australia. The black box marks the  
404 area shown in Figure 1b. (b) Zoom-in map of the study area showing the location of the city of  
405 Portland and the Otway Basin. The white lines represent 2D seismic reflection data, the black  
406 dotted line represents the location of the modern shelf edge and the inferred location of the

407 Miocene continental shelf edge (modified from Leach and Wallace, 2001), and the red box  
408 represents the extent of the 3D seismic reflection dataset. The GEBCO\_2014 bathymetry map is  
409 downloaded from <https://www.ngdc.noaa.gov/maps/autogrid/>.

410 Figure 2. Stratigraphic and tectonic event chart for the study area, showing the key horizons  
411 mapped in the seismic data and major tectonic events in the study interval. This figure is modified  
412 from Krassay et al. (2004) and Perincek and Cockshell (1995). The Horizon H1 has been correlated  
413 to the late-Cretaceous unconformity surface from Holford et al. (2014). The Horizon H2 has been  
414 correlated to the late-Miocene unconformity surface from Hillis et al. (2008).

415 Figure 3. Large scale regional seismic section across the inner SE Australian shelf to the deeper  
416 abyssal plain, highlighting Unconformity surface (H1), and basinward thickening of the Upper  
417 Cretaceous supersequence. See the location of this regional seismic profile in Figure 1b. Figure 3 is  
418 originally downloaded and modified from Geoscience Australia official website  
419 (<https://www.ga.gov.au/scientific-topics>).

420 Figure 4. (a) W-E seismic cross-section through the 3D seismic data area (see Figure 1b for location).  
421 (b) Interpreted seismic cross-section, showing the key horizons, major faults, and the location of  
422 the buried canyons.

423 Figure 5. (a) N-S seismic dip-section through the 3D seismic data area (see Figure 1b for location).  
424 (b) Interpreted seismic dip-section, showing the key horizons and the major faults.

425 Figure 6. Seismic facies classification figure.

426 Figure 7. (a) Depth structure map of Horizon H2 within OS02 3D area. (b) interpreted sketch of  
427 Figure 7a, showing the morphology of Buried canyons (BC-1 and BC-2).

428 Figure 8. (a) Seismic section cutting across the Upper Segment of the BC-1, showing the location  
429 of BC-1 and Horizons H1 and H2. (b) Seismic section cutting across the Upper Segment of the BC-  
430 1, showing the location of BC-1 and Horizons H1 and H2. (c) Seismic section cutting across the  
431 Lower Segment of the BC-1, showing the location of BC-1 and BC-2, and Horizons H1 and H2. (d)  
432 Seismic section cutting across the Lower Segment of the BC-1, showing the location of BC-1 and  
433 BC-2, and Horizons H1 and H2. See the location of this figure in Figure 7b, and see the uninterpreted,  
434 clean seismic sections in the supplementary material.

435 Figure 9. (a) 2D seismic section in the deep submarine settings showing the cross-section of the  
436 buried canyons. (b) 2D seismic section in the deep submarine settings showing the dip-section of

437 the buried canyons. See location of this figure from Figure 1b, and see the uninterpreted, clean  
438 seismic sections in the supplementary material.

439 Figure 10. (a) Variance attribute calculated on horizon H2.1, showing a map view of MTC-1. Note  
440 that the white dotted lines indicate the boundary of the buried canyon, and the yellow dotted lines  
441 indicate the boundary of MTCs. (b) Variance attribute calculated on horizon H2.2, showing a map  
442 view of MTC-2. (c) Variance attribute calculated on horizon H2.3, showing the map view of MTC-3.  
443 See the location of this figure in Figure 7b.

444 Figure 11. (a) Variance attribute map calculated on the horizon a (see the location of this horizon  
445 in Figure 11c), showing the extensional faults formed during the Late Cretaceous. (b). Interpreted  
446 view of Figure 11a, showing the location of the extensional faults (white dotted lines) and the  
447 location of the buried canyons (blue dotted lines). (c) Seismic cross-section through the area  
448 outside of the buried canyons (see Figure 11b for location). See the uninterpreted Figure 11c in the  
449 supplementary material.

450 Figure 12. Schematic figure showing the evolution model of the buried canyons. (a) Schematic  
451 figure showing that the regionally distributed, Late Cretaceous extensional faults. (b) Schematic  
452 figure showing the initiation of the MTCs that formed the canyon bases during the Late Miocene.  
453 (c) Schematic figure showing the canyon-fill pattern after the formation of the canyon base.

## 454 Data Access

455 The data used in this study can be requested from the Geoscience Australia Repository  
456 <https://www.ga.gov.au/data-pubs>. In this study we used OS02 3D survey and OS02 2D survey. The  
457 GEBCO\_2014 bathymetry map is downloaded from <https://www.ngdc.noaa.gov/maps/autogrid/>.

## 458 Acknowledgements

459 The authors would like to thank Geoscience Australia for providing the seismic reflection data used  
460 in this study. The first and the third author thanks the State Key Laboratory of Marine Geology for  
461 its financial support.

462 Reference

- 463 Antobreh, A.A., Krastel, S., 2006. Morphology, seismic characteristics and development of Cap Timiris  
464 Canyon, offshore Mauritania: a newly discovered canyon preserved-off a major arid climatic region.  
465 *Marine and Petroleum Geology* 23, 37-59.
- 466 Baztan, J., Berné, S., Olivet, J.-L., Rabineau, M., Aslanian, D., Gaudin, M., Réhault, J.-P., Canals, M., 2005.  
467 Axial incision: The key to understand submarine canyon evolution (in the western Gulf of Lion). *Marine*  
468 *and Petroleum Geology* 22, 805-826.
- 469 Brown, A.R., 2011. Interpretation of three-dimensional seismic data. Society of Exploration  
470 Geophysicists and American Association of Petroleum Geologists.
- 471 Bull, S., Cartwright, J., Huuse, M., 2009. A review of kinematic indicators from mass-transport complexes  
472 using 3D seismic data. *Marine and Petroleum Geology* 26, 1132-1151.
- 473 Butler, R.W., Eggenhuisen, J.T., Haughton, P., McCaffrey, W.D., 2016. Interpreting syndepositional  
474 sediment remobilization and deformation beneath submarine gravity flows; a kinematic boundary layer  
475 approach. *Journal of the Geological Society* 173, 46-58.
- 476 Champion, K.M., Sprague, A., Mohrig, D., Lovell, R., Drzewiecki, P., Sullivan, M., Ardill, J., Jensen, G.,  
477 Sickafoose, D., 2003. Outcrop expression of confined channel complexes.
- 478 Coleman, J.M., Prior, D.B., Lindsay, J.F., 1983. Deltaic influences on shelfedge instability processes.
- 479 Cross, N.E., Cunningham, A., Cook, R.J., Taha, A., Esmatie, E., El Swidan, N., 2009. Three-dimensional  
480 seismic geomorphology of a deep-water slope-channel system: The Sequoia field, offshore west Nile  
481 Delta, Egypt. *AAPG bulletin* 93, 1063-1086.
- 482 Crossey, L.J., Fischer, T.P., Patchett, P.J., Karlstrom, K.E., Hilton, D.R., Newell, D.L., Huntoon, P., Reynolds,  
483 A.C., De Leeuw, G.A., 2006. Dissected hydrologic system at the Grand Canyon: Interaction between  
484 deeply derived fluids and plateau aquifer waters in modern springs and travertine. *Geology* 34, 25-28.
- 485 Deptuck, M.E., Sylvester, Z., Pirmez, C., O'Byrne, C., 2007. Migration-aggradation history and 3-D  
486 seismic geomorphology of submarine channels in the Pleistocene Benin-major Canyon, western Niger  
487 Delta slope. *Marine and Petroleum Geology* 24, 406-433.
- 488 Di Celma, C., 2011. Sedimentology, architecture, and depositional evolution of a coarse-grained  
489 submarine canyon fill from the Gelasian (early Pleistocene) of the Peri-Adriatic basin, Offida, central  
490 Italy. *Sedimentary Geology* 238, 233-253.
- 491 Dickinson, J., Wallace, M., Holdgate, G., Daniels, J., Gallagher, S., Thomas, L., 2001. Neogene tectonics  
492 in SE Australia: implications for petroleum systems. *The APPEA Journal* 41, 37-52.
- 493 Dickinson, J.A., Wallace, M.W., Holdgate, G.R., Gallagher, S.J., Thomas, L., 2002. Origin and timing of the  
494 Miocene-Pliocene unconformity in southeast Australia. *Journal of Sedimentary Research* 72, 288-303.
- 495 Duddy, I., 1997. Focussing exploration in the Otway Basin: understanding timing of source rock  
496 maturation. *The APPEA Journal* 37, 178-191.
- 497 Eyles, C.H., Lagoe, M.B., 1998. Slump-generated megachannels in the Pliocene-Pleistocene  
498 glaciomarine Yakataga Formation, Gulf of Alaska. *Geological Society of America Bulletin* 110, 395-408.
- 499 Figueiredo, J.J., Hodgson, D.M., Flint, S.S., Kavanagh, J.P., 2013. Architecture of a channel complex  
500 formed and filled during long-term degradation and entrenchment on the upper submarine slope, Unit  
501 F, Fort Brown Fm., SW Karoo Basin, South Africa. *Marine and Petroleum Geology* 41, 104-116.
- 502 Gong, C., Wang, Y., Zhu, W., Li, W., Xu, Q., Zhang, J., 2011. The Central Submarine Canyon in the  
503 Qiongdongnan Basin, northwestern South China Sea: architecture, sequence stratigraphy, and

504 depositional processes. *Marine and Petroleum Geology* 28, 1690-1702.

505 Goodwin, R.H., Prior, D.B., 1989. Geometry and depositional sequences of the Mississippi Canyon, Gulf  
506 of Mexico. *Journal of Sedimentary Research* 59, 318-329.

507 Green, P., Crowhurst, P., Duddy, I., 2004. Integration of AFTA and (U-Th)/He thermochronology to  
508 enhance the resolution and precision of thermal history reconstruction in the Anglesea-1 well, Otway  
509 Basin, SE Australia.

510 He, Y., Xie, X., Kneller, B.C., Wang, Z., Li, X., 2013. Architecture and controlling factors of canyon fills on  
511 the shelf margin in the Qiongdongnan Basin, northern South China Sea. *Marine and Petroleum Geology*  
512 41, 264-276.

513 He, Y., Zhong, G., Wang, L., Kuang, Z., 2014. Characteristics and occurrence of submarine canyon-  
514 associated landslides in the middle of the northern continental slope, South China Sea. *Marine and*  
515 *Petroleum Geology* 57, 546-560.

516 Hill, K.C., Hill, K.A., Cooper, G.T., O'Sullivan, A.J., O'Sullivan, P.B., Richardson, M.J., 1995. Inversion around  
517 the Bass basin, SE Australia. *Geological Society, London, Special Publications* 88, 525-547.

518 Hillis, R.R., Sandiford, M., Reynolds, S.D., Quigley, M.C., 2008. Present-day stresses, seismicity and  
519 Neogene-to-Recent tectonics of Australia's 'passive' margins: intraplate deformation controlled by plate  
520 boundary forces. *Geological Society, London, Special Publications* 306, 71-90.

521 Hodgson, D., Di Celma, C., Brunt, R., Flint, S., 2011. Submarine slope degradation and aggradation and  
522 the stratigraphic evolution of channel–levee systems. *Journal of the Geological Society* 168, 625-628.

523 Holdgate, G., Wallace, M., Gallagher, J.D.S., Keene, J., Smith, A., 2000. Controls on Seaspray Group sonic  
524 velocities in the Gippsland Basin—a multi-disciplinary approach to the canyon seismic velocity problem.  
525 *The APPEA Journal* 40, 293-313.

526 Holford, S.P., Tuit, A.K., Hillis, R.R., Green, P.F., Stoker, M.S., Duddy, I.R., Sandiford, M., Tassone, D.R.,  
527 2014. Cenozoic deformation in the Otway Basin, southern Australian margin: Implications for the origin  
528 and nature of post-breakup compression at rifted margins. *Basin Research* 26, 10-37.

529 Krassay, A., Cathro, D., Ryan, D., 2004. A regional tectonostratigraphic framework for the Otway Basin.

530 Leach, A., Wallace, M., 2001. Cenozoic submarine canyon systems in cool water carbonates from the  
531 Otway Basin, Victoria, Australia.

532 Lewis, K.B., Barnes, P.M., 1999. Kaikoura Canyon, New Zealand: active conduit from near-shore  
533 sediment zones to trench-axis channel. *Marine Geology* 162, 39-69.

534 Liang, C., Xie, X., He, Y., Chen, H., Yu, X., Zhang, W., Mi, H., Lu, B., Tian, D., Zhang, H., 2020. Multiple  
535 sediment sources and topographic changes controlled the depositional architecture of a palaeoslope-  
536 parallel canyon in the Qiongdongnan Basin, South China Sea. *Marine and Petroleum Geology* 113,  
537 104161.

538 Maier, K.L., Johnson, S.Y., Hart, P., 2018. Controls on submarine canyon head evolution: Monterey  
539 Canyon, offshore central California. *Marine Geology* 404, 24-40.

540 Mauffrey, M.-A., Urgeles, R., Berné, S., Canning, J., 2017. Development of submarine canyons after the  
541 Mid-Pleistocene Transition on the Ebro margin, NW Mediterranean: The role of fluvial connections.  
542 *Quaternary Science Reviews* 158, 77-93.

543 Mayall, M., Jones, E., Casey, M., 2006. Turbidite channel reservoirs—Key elements in facies prediction  
544 and effective development. *Marine and Petroleum Geology* 23, 821-841.

545 McGowran, B., Holdgate, G., Li, Q., Gallagher, S., 2004. Cenozoic stratigraphic succession in southeastern  
546 Australia. *Australian Journal of Earth Sciences* 51, 459-496.

547 Moore, A., Stagg, H., Norvick, M., 2000. Deep-water Otway Basin: a new assessment of the tectonics

548 and hydrocarbon prospectivity. *The APPEA Journal* 40, 66-85.

549 Normark, W.R., Carlson, P.R., Chan, M., Archer, A., 2003. Giant submarine canyons: Is size any clue to  
550 their importance in the rock record? *Special Papers-Geological Society of America*, 175-190.

551 Norvick, M., Smith, M., 2001. Mapping the plate tectonic reconstruction of southern and southeastern  
552 Australia and implications for petroleum systems. *The APPEA Journal* 41, 15-35.

553 Perincek, D., Cockshell, C., 1995. The Otway basin: early Cretaceous rifting to Neogene inversion. *The*  
554 *APPEA Journal* 35, 451-466.

555 Perov, G., Bhattacharya, J.P., 2011. Pleistocene shelf-margin delta: Intradeltaic deformation and  
556 sediment bypass, northern Gulf of Mexico. *AAPG bulletin* 95, 1617-1641.

557 Posamentier, H., Erskine, R., Mitchum, R., 1991. Models for submarine-fan deposition within a  
558 sequence-stratigraphic framework, Seismic facies and sedimentary processes of submarine fans and  
559 turbidite systems. Springer, pp. 127-136.

560 Posamentier, H.W., 2005. Stratigraphy and geomorphology of deep-water mass transport complexes  
561 based on 3D seismic data, SEG Technical Program Expanded Abstracts 2005. Society of Exploration  
562 Geophysicists, pp. 2300-2303.

563 Posamentier, H.W., Kolla, V., 2003. Seismic geomorphology and stratigraphy of depositional elements in  
564 deep-water settings. *Journal of sedimentary research* 73, 367-388.

565 Prather, B.E., Booth, J.R., Steffens, G.S., Craig, P.A., 1998. Classification, lithologic calibration, and  
566 stratigraphic succession of seismic facies of intraslope basins, deep-water Gulf of Mexico. *AAPG bulletin*  
567 82, 701-728.

568 Pratson, L.F., Coakley, B.J., 1996. A model for the headward erosion of submarine canyons induced by  
569 downslope-eroding sediment flows. *Geological Society of America Bulletin* 108, 225-234.

570 Qin, Y., Alves, T.M., Constantine, J., Gamboa, D., 2017. The role of mass wasting in the progressive  
571 development of submarine channels (Espírito Santo Basin, SE Brazil). *Journal of Sedimentary Research*  
572 87, 500-516.

573 Rasmussen, E.S., 1994. The relationship between submarine canyon fill and sea-level change: an  
574 example from Middle Miocene offshore Gabon, West Africa. *Sedimentary Geology* 90, 61-75.

575 Rebesco, M., Hernández-Molina, F.J., Van Rooij, D., Wåhlin, A., 2014. Contourites and associated  
576 sediments controlled by deep-water circulation processes: State-of-the-art and future considerations.  
577 *Marine Geology* 352, 111-154.

578 Sandiford, M., 2003. Neotectonics of southeastern Australia: linking the Quaternary faulting record with  
579 seismicity and in situ stress. *Special Papers-geological Society of America*, 107-120.

580 Sandiford, M., 2007. The tilting continent: a new constraint on the dynamic topographic field from  
581 Australia. *Earth and Planetary Science Letters* 261, 152-163.

582 Sandiford, M., Wallace, M., Coblenz, D., 2004. Origin of the in situ stress field in south-eastern Australia.  
583 *Basin Research* 16, 325-338.

584 Sequeiros, O.E., Pittaluga, M.B., Frascati, A., Pirmez, C., Masson, D.G., Weaver, P., Crosby, A.R., Lazzaro,  
585 G., Botter, G., Rimmer, J.G., 2019. How typhoons trigger turbidity currents in submarine canyons.  
586 *Scientific reports* 9, 1-15.

587 Shepard, F.P., 1981. Submarine canyons: multiple causes and long-time persistence. *AAPG bulletin* 65,  
588 1062-1077.

589 Shepard, F.P., Marshall, N.F., McLoughlin, P.A., 1974. " Internal Waves" Advancing along Submarine  
590 Canyons. *Science* 183, 195-198.

591 Stow, D., Faugères, J.-C., 2008. Contourite facies and the facies model. *Developments in sedimentology*

592 60, 223-256.

593 Stow, D.A., Faugères, J.-C., Howe, J.A., Pudsey, C.J., Viana, A.R., 2002. Bottom currents, contourites and  
594 deep-sea sediment drifts: current state-of-the-art. Geological Society, London, Memoirs 22, 7-20.

595 Su, M., Lin, Z., Wang, C., Kuang, Z., Liang, J., Chen, H., Liu, S., Zhang, B., Luo, K., Huang, S., 2020.  
596 Geomorphologic and infilling characteristics of the slope-confined submarine canyons in the Pearl River  
597 Mouth Basin, northern South China Sea. Marine Geology 424, 106166.

598 Su, M., Xie, X., Xie, Y., Wang, Z., Zhang, C., Jiang, T., He, Y., 2014. The segmentations and the significances  
599 of the Central Canyon System in the Qiongdongnan Basin, northern South China Sea. Journal of Asian  
600 Earth Sciences 79, 552-563.

601 Symons, W.O., Sumner, E.J., Paull, C.K., Cartigny, M.J., Xu, J., Maier, K.L., Lorenson, T.D., Talling, P.J., 2017.  
602 A new model for turbidity current behavior based on integration of flow monitoring and precision coring  
603 in a submarine canyon. Geology 45, 367-370.

604 Tassone, D., Holford, S., Tingay, M., Tuitt, A., Stoker, M., Hillis, R., 2011. Overpressures in the central  
605 Otway Basin: the result of rapid Pliocene–Recent sedimentation? The APPEA Journal 51, 439-458.

606 Tassone, D.R., Holford, S.P., Duddy, I.R., Green, P.F., Hillis, R.R., 2014. Quantifying Cretaceous–Cenozoic  
607 exhumation in the Otway Basin, southeastern Australia, using sonic transit time data: Implications for  
608 conventional and unconventional hydrocarbon prospectivity. AAPG Bulletin 98, 67-117.

609 Tassone, D.R., Holford, S.P., Hillis, R.R., Tuitt, A.K., 2012. Quantifying Neogene plate-boundary controlled  
610 uplift and deformation of the southern Australian margin. Geological Society, London, Special  
611 Publications 367, 91-110.

612 Totterdell, J., Bradshaw, M., Owen, K., Hashimoto, T., Hall, L., 2014. Petroleum geology inventory of  
613 Australia's offshore frontier basins. Geoscience Australia.

614 Van Bommel, P.P., Pepper, R.E., 2000. Seismic signal processing method and apparatus for generating a  
615 cube of variance values. Google Patents.

616 Warratz, G., Schwenk, T., Voigt, I., Bozzano, G., Henrich, R., Violante, R., Lantzsch, H., 2019. Interaction  
617 of a deep-sea current with a blind submarine canyon (Mar del Plata Canyon, Argentina). Marine Geology  
618 417, 106002.

619 Willcox, J., Stagg, H., 1990. Australia's southern margin: a product of oblique extension. Tectonophysics  
620 173, 269-281.

621 Wu, N., Jackson, C.A.-L., Johnson, H.D., Hodgson, D.M., 2021a. Lithological, petrophysical, and seal  
622 properties of mass-transport complexes, northern Gulf of Mexico. AAPG Bulletin 105, 1461-1489.

623 Wu, N., Nugraha, H.D., Zhong, F.G., Steventon, M., 2021b. The role of mass-transport complexes (MTCs)  
624 in the initiation and evolution of submarine canyons.

625 Zecchin, M., Caffau, M., Roda, C., 2011. Relationships between high-magnitude relative sea-level  
626 changes and filling of a coarse-grained submarine canyon (Pleistocene, Ionian Calabria, Southern Italy).  
627 Sedimentology 58, 1030-1064.

628 Ziesch, J., Aruffo, C.M., Tanner, D.C., Beilecke, T., Dance, T., Henk, A., Weber, B., Tenthorey, E., Lippmann,  
629 A., Krawczyk, C.M., 2017. Geological structure and kinematics of normal faults in the Otway Basin,  
630 Australia, based on quantitative analysis of 3-D seismic reflection data. Basin Research 29, 129-148.

631

Figure 1

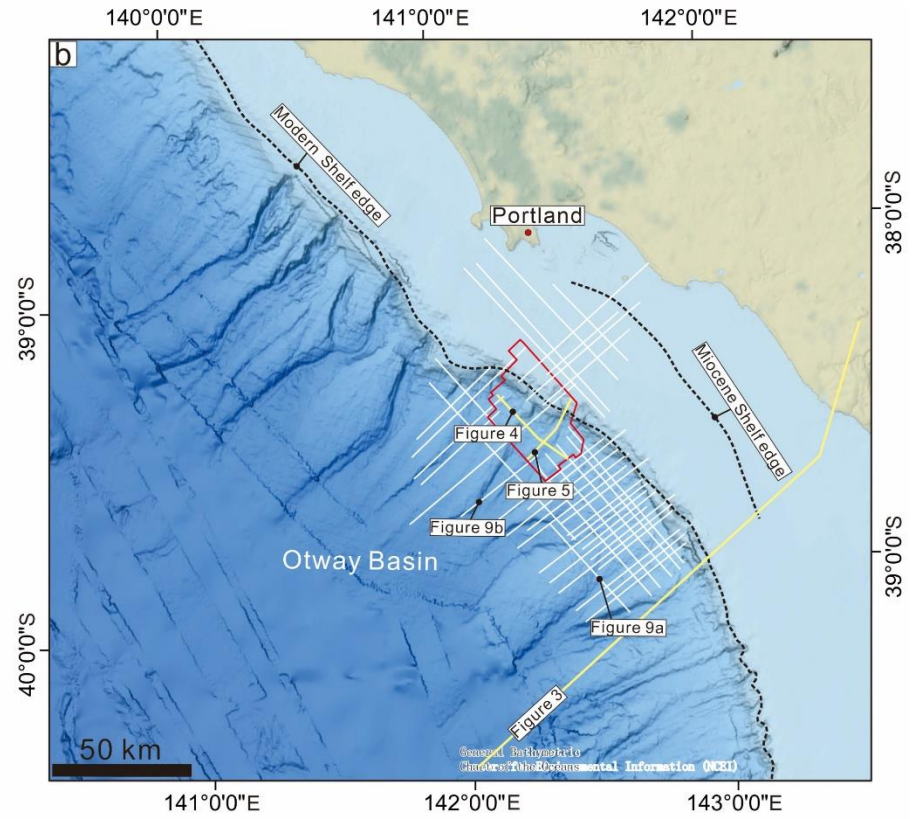
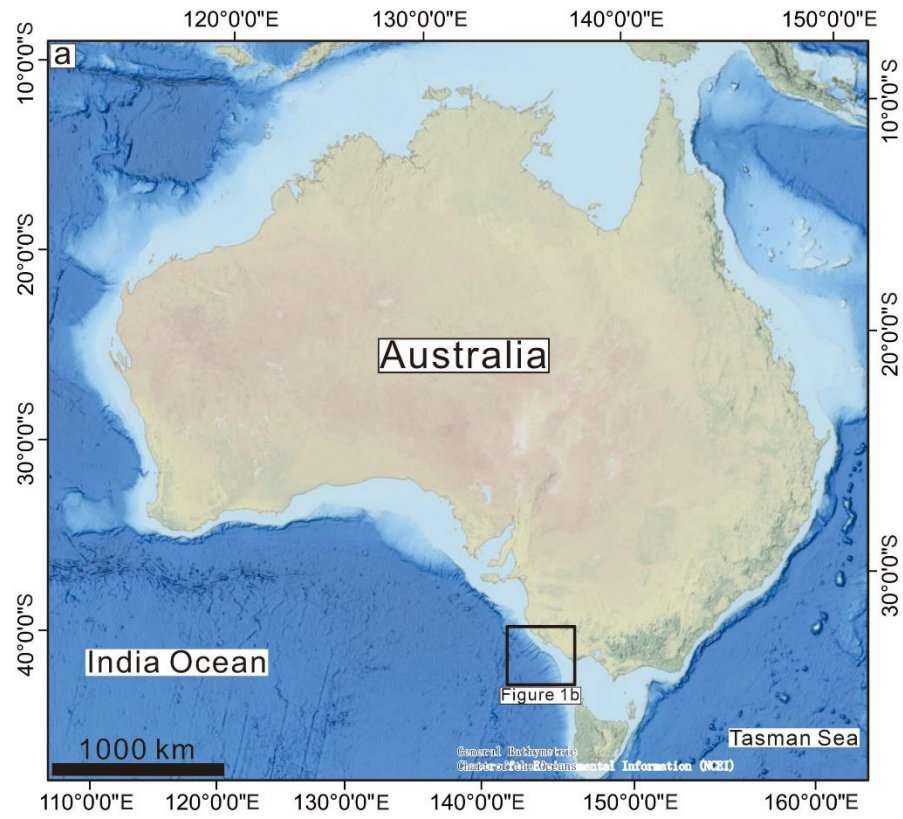


Figure 2

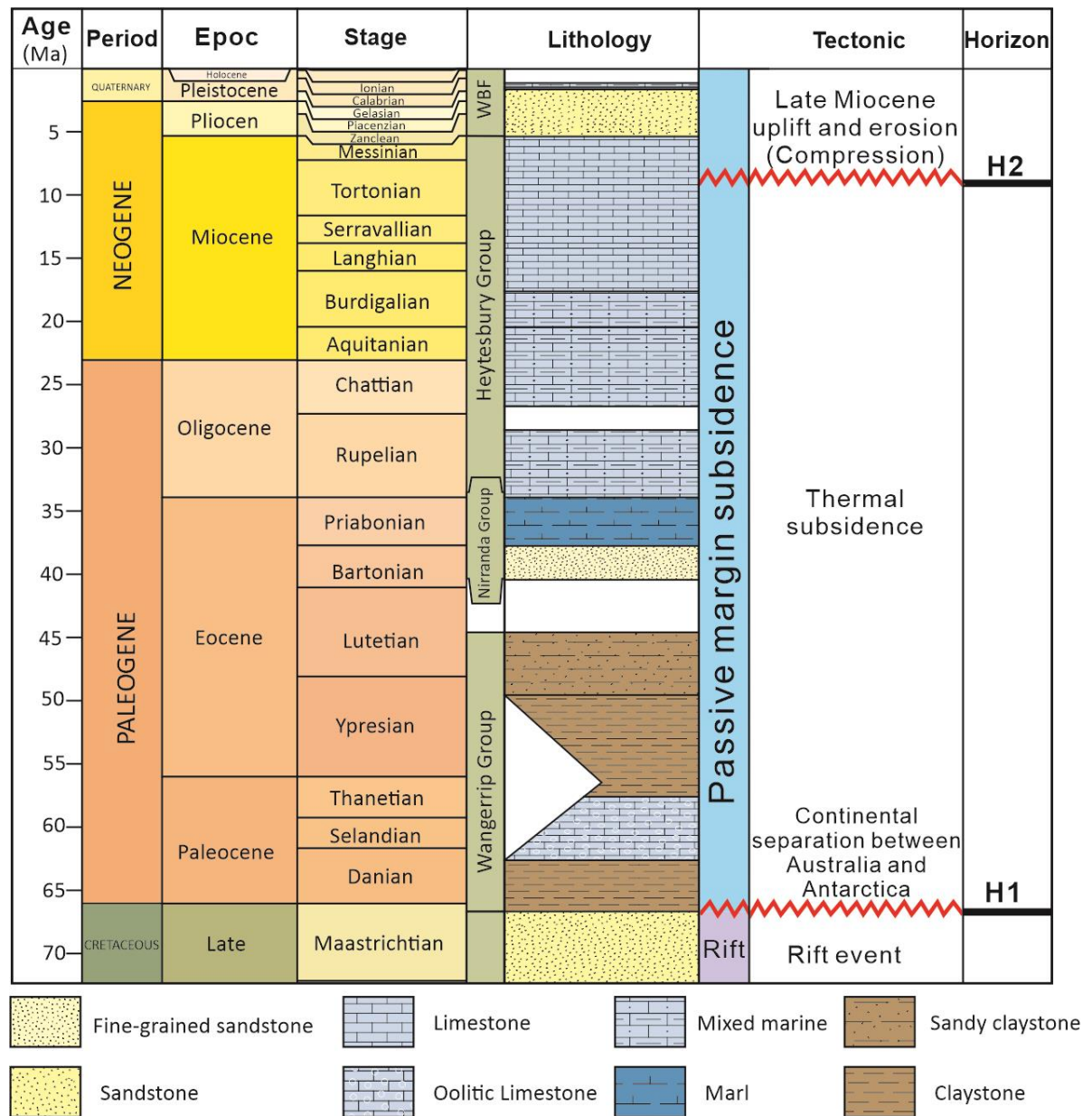


Figure 3

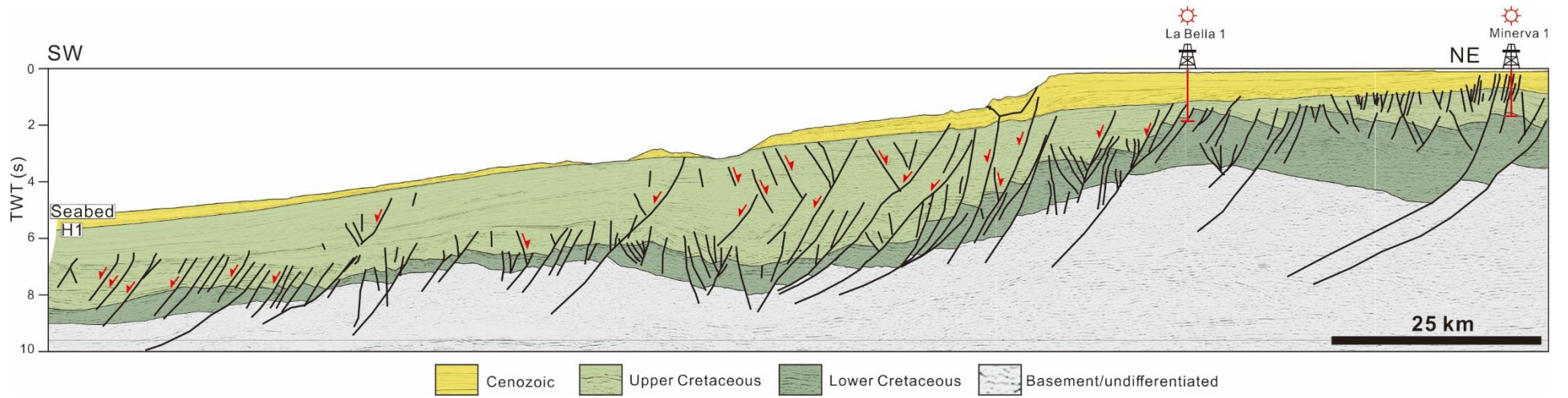


Figure 4

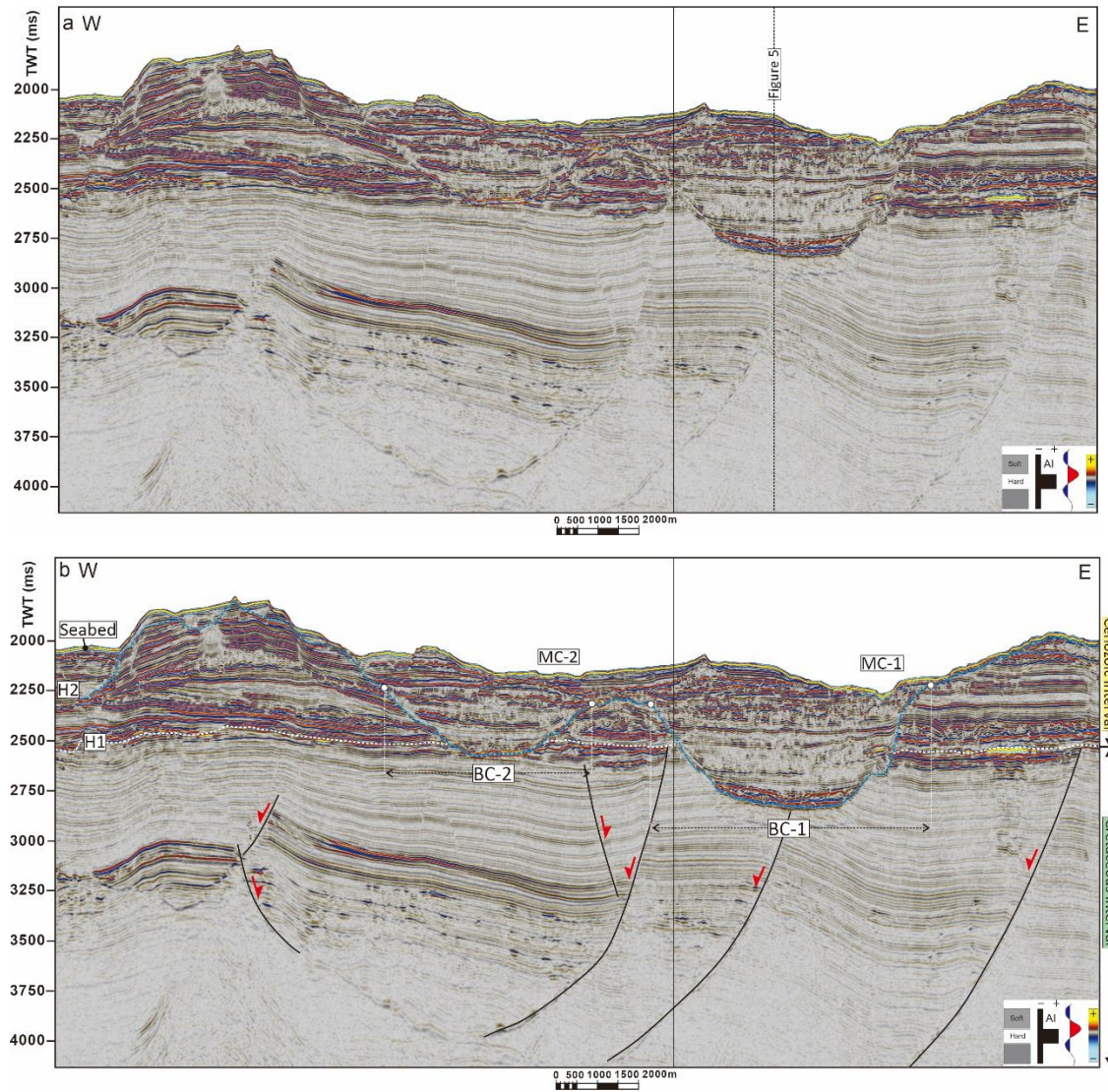


Figure 5

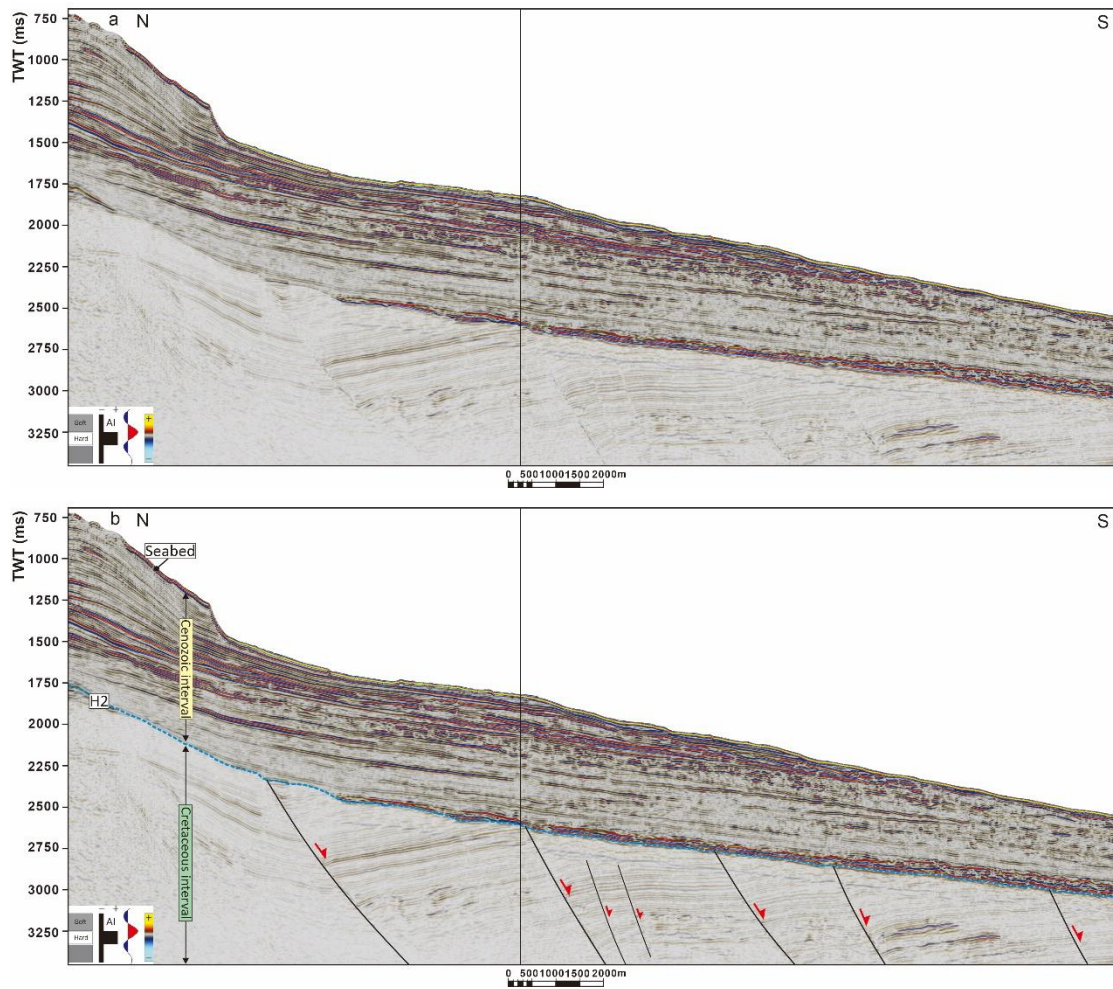


Figure 6

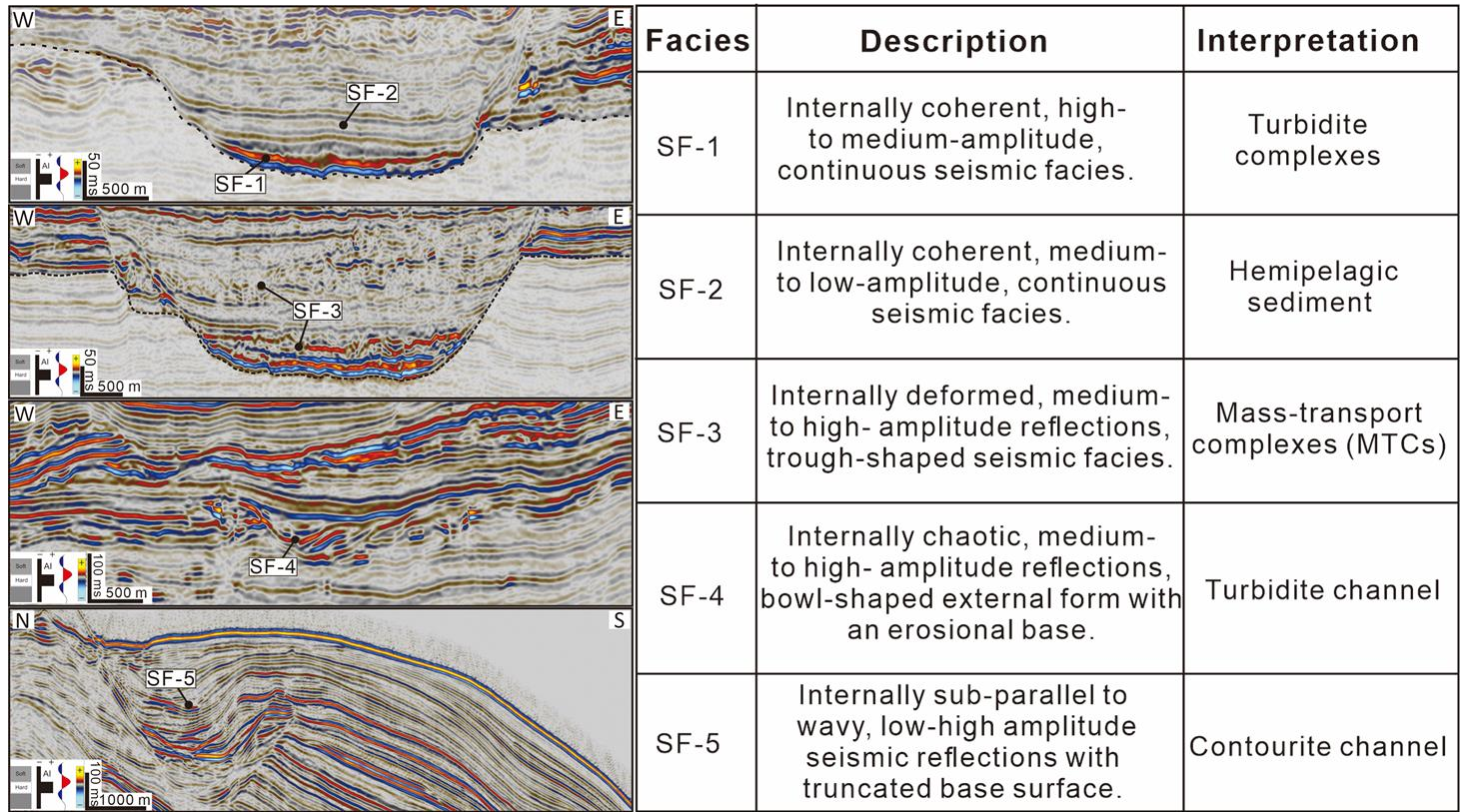


Figure 7

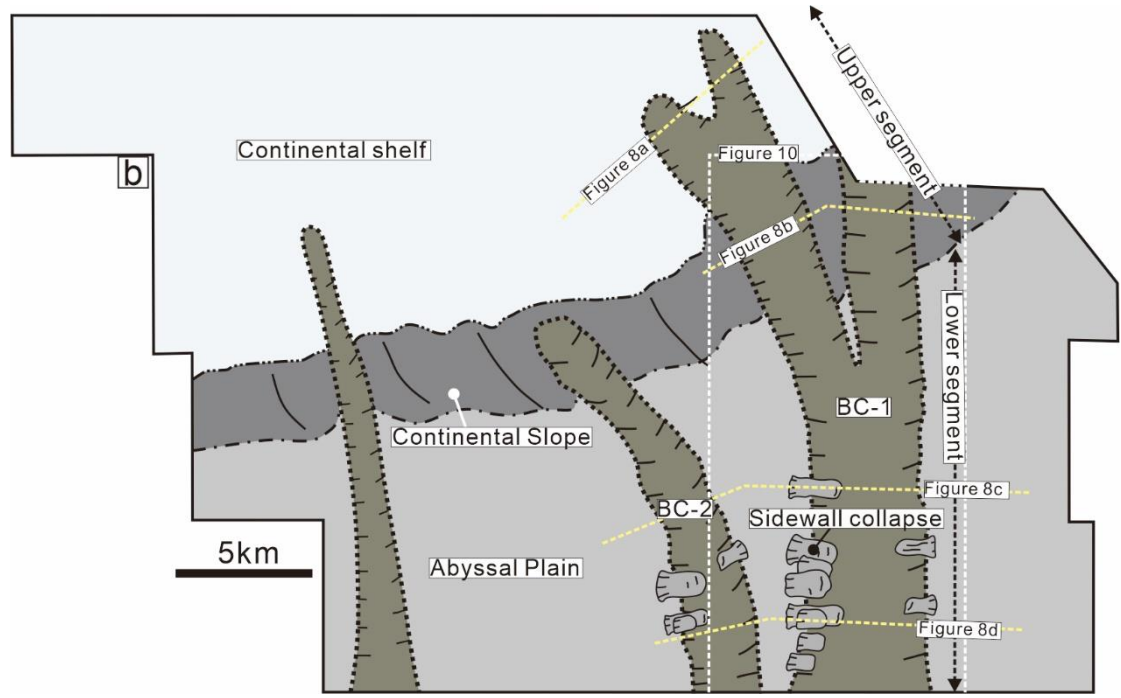
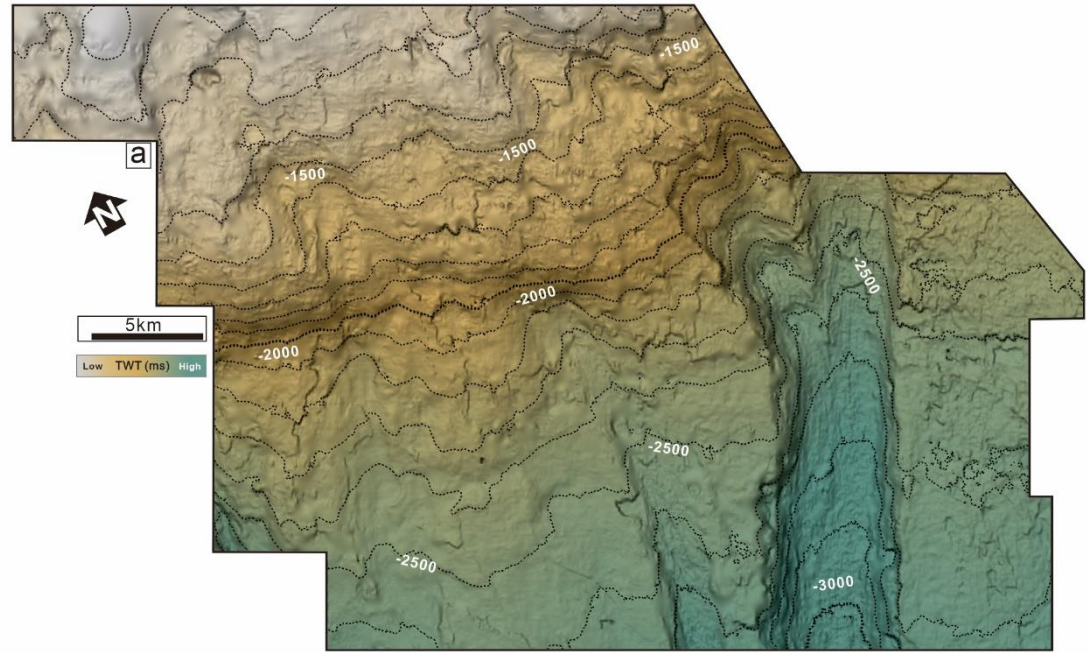


Figure 8

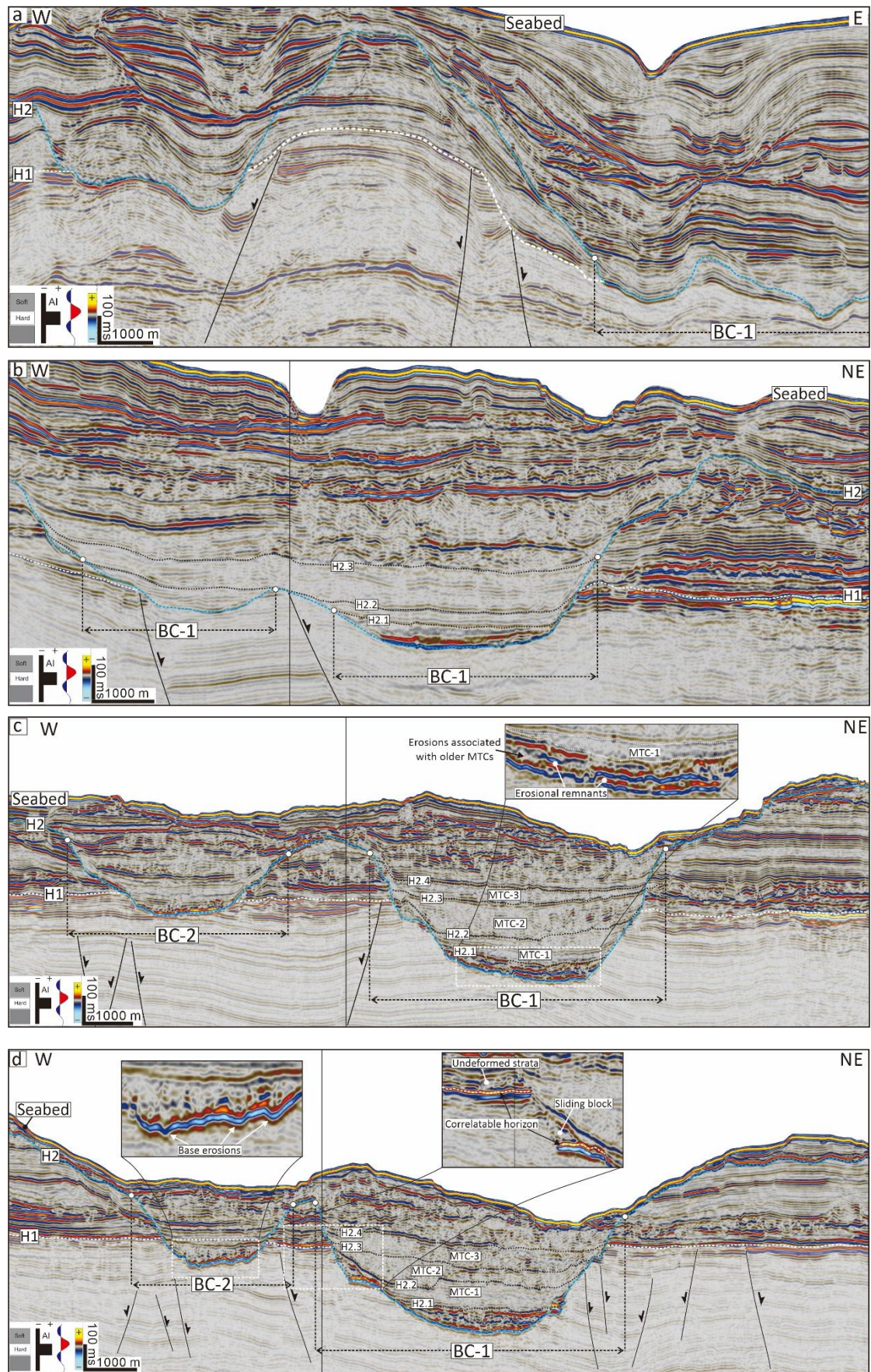


Figure 9

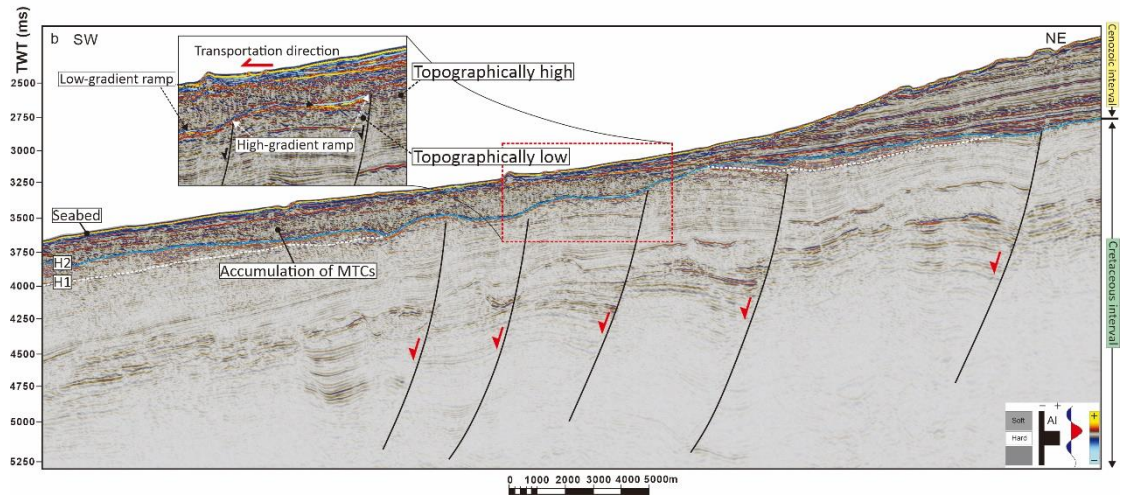
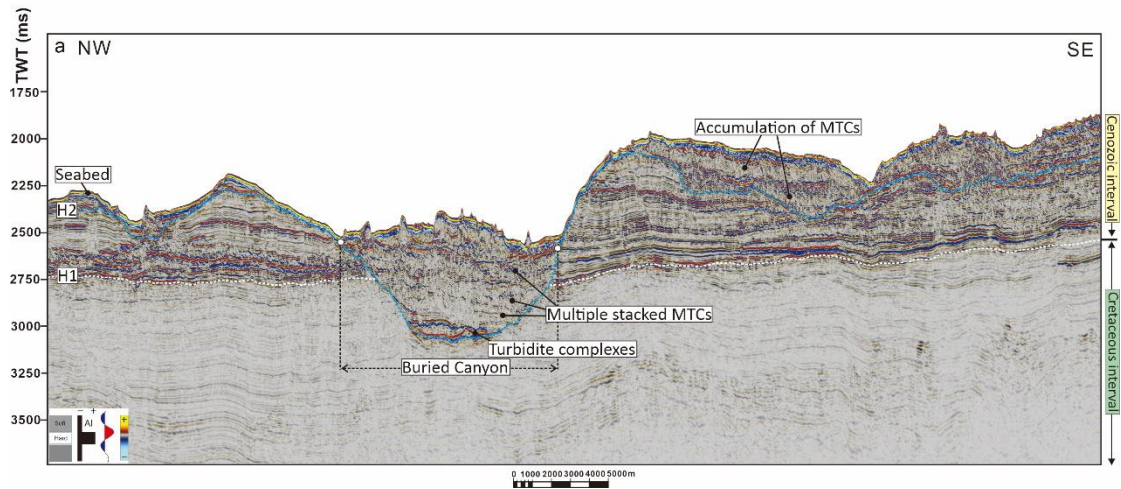


Figure 10

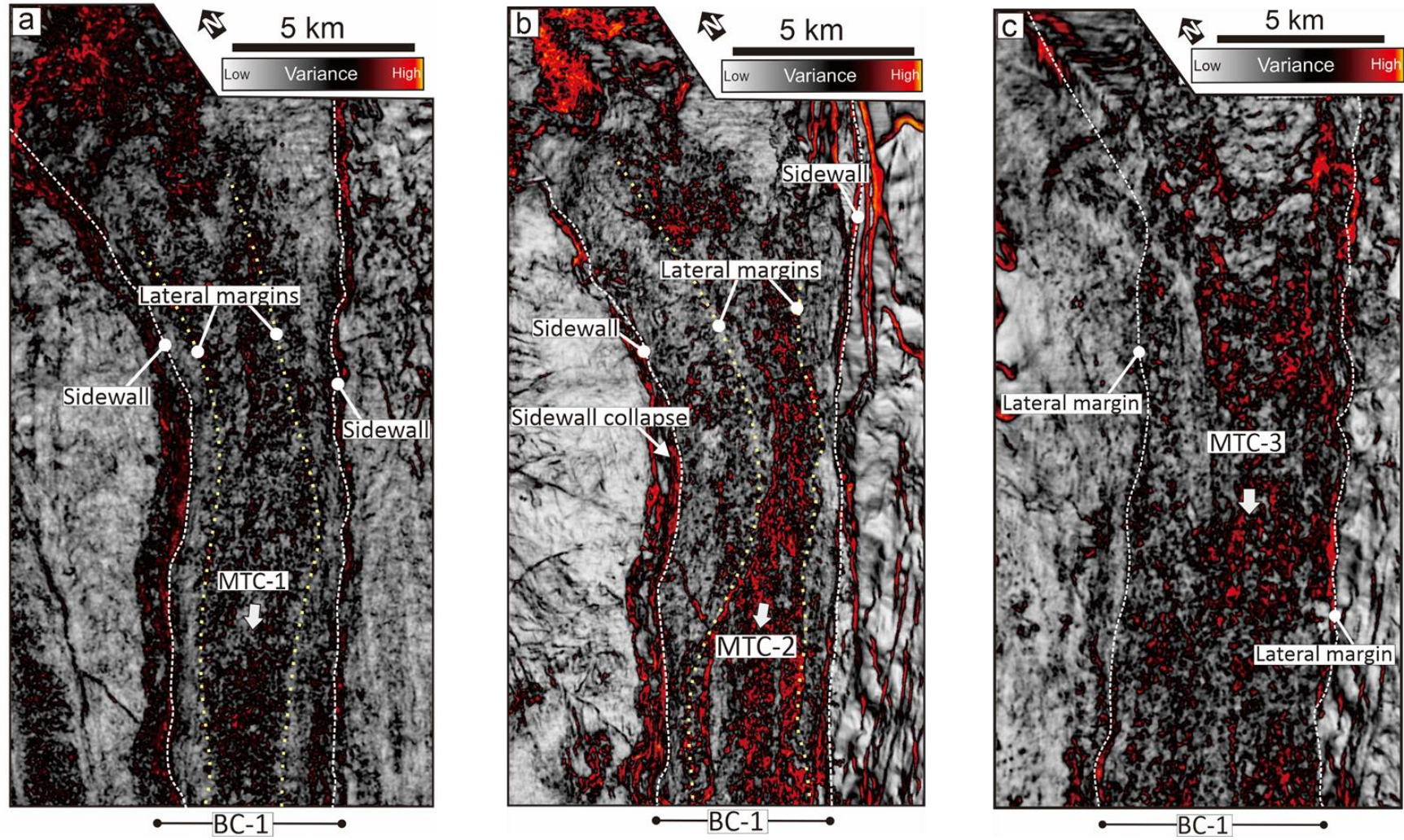
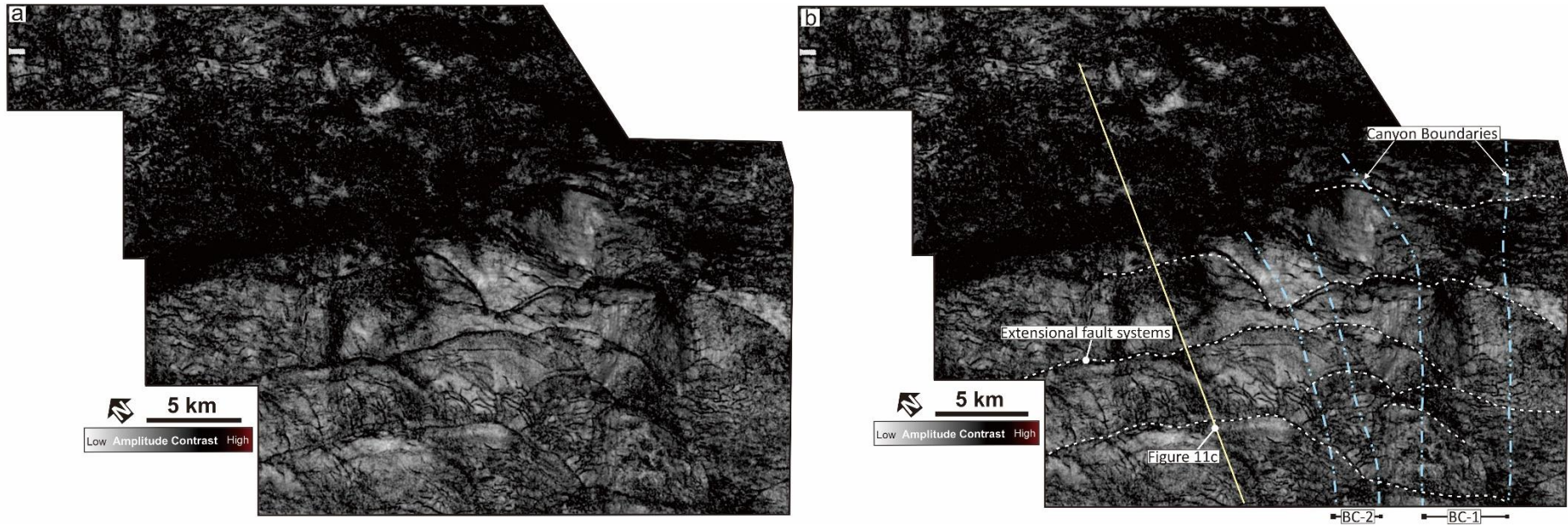


Figure 11



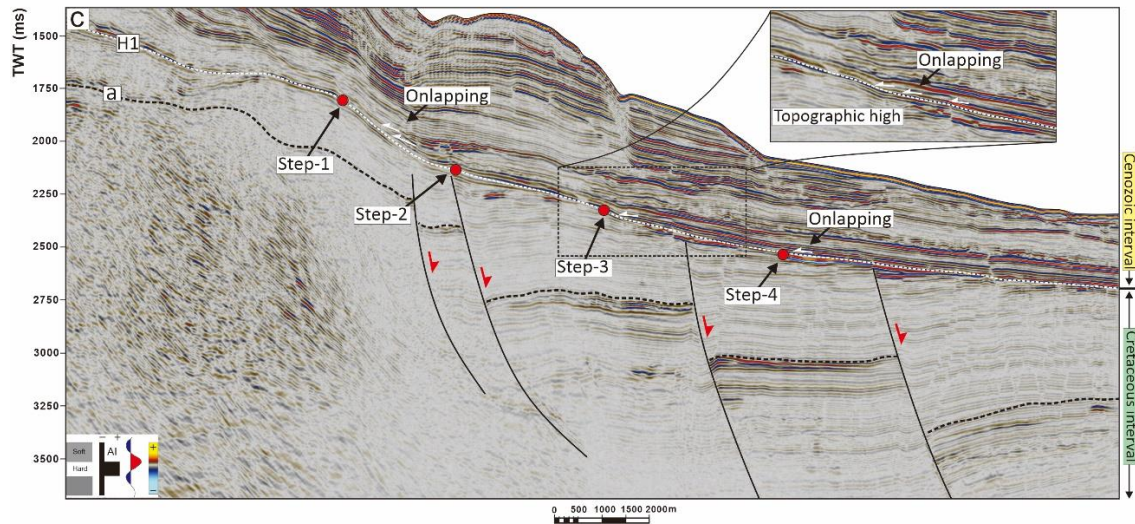
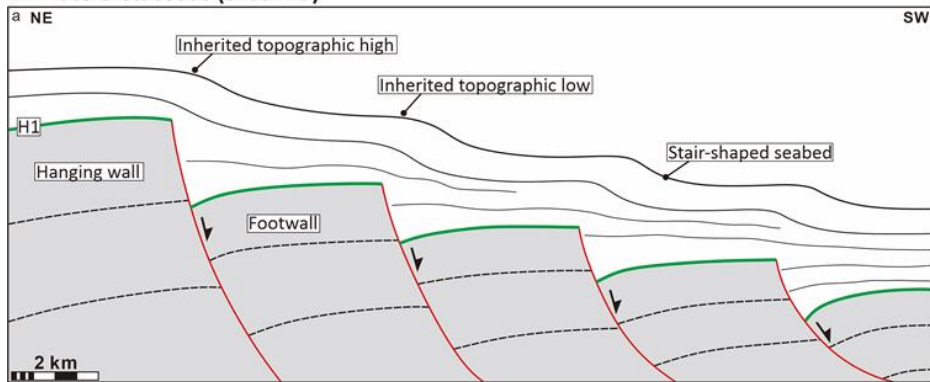
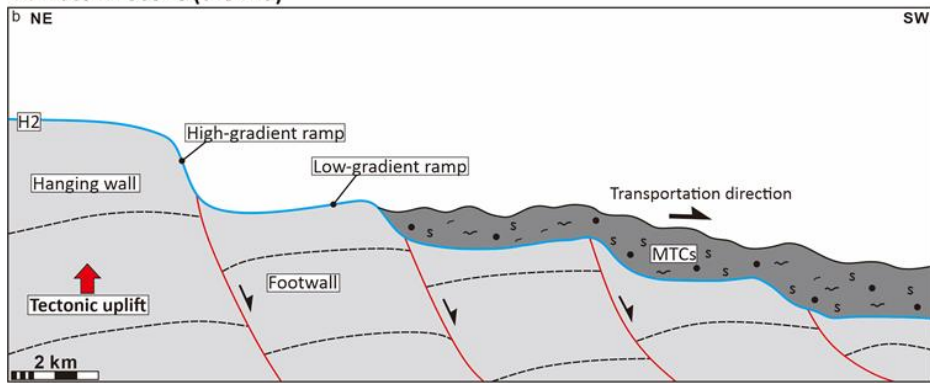


Figure 12

**T1: Late Cretaceous (c. 65 Ma)**



**T2: Late Miocene (c. 5 Ma)**



**T3: Post Late Miocene**

